Sidelobe Reductions in Linear Array Antennas Using Electronically Displaced Phase Center Antenna Technique

Tanzeela Mitha, *Student Member, IEEE*, Maria Pour, *Senior Member, IEEE*

***Abstract*—A novel approach to sidelobe reduction in uniformly-excited, equally-spaced linear arrays using the electronically displaced phase center antenna (E-DPCA) technique is presented for the first time. Antenna elements with the E-DPCA capability are employed in 9- and 21-element linear array antennas for the proof of concept. The element spacing of these physically periodic arrays is electronically tapered by displacing the phase center location, and thus the relative coordinates, of the base elements to reduce the sidelobe and minor lobe levels. Compared to the pre-existing synthesis techniques, the proposed technique provides not only comparable sidelobe reductions but also an additional capability of adaptively changing the array configuration to generate desired patterns without any physical means, while maintaining the same overall array length.**

***Index Terms*—Phased arrays, sidelobe level (SLL), aperiodic array, electronically displaced phase center antenna (E-DPCA)**

I. Introduction

A number of synthesis techniques have been developed in the past few decades to control and modify the radiation pattern characteristics of array antennas in radars, satellite communications, navigation, and remote sensing. Equally-spaced arrays often employ amplitude [1-3] and phase [4,5] excitation techniques to generate radiation patterns with low sidelobe levels (SLLs). In aperiodic arrays, SLLs are reduced by varying the density of uniformly-excited elements or unequally distributing the position of the base elements [6-20] or by array thinning in large antennas [21-24]. A variety of evolutionary algorithms have been developed to determine the optimal position of the elements in aperiodic arrays to reduce sidelobe and minor lobe levels [12-20]. However, once the element position is fixed, the array configuration generates a modified pattern that satisfies only one requirement at a time. In order to further adapt the pattern for other requirements, the base elements need to be physically rearranged into different periodic or aperiodic configurations. This burdensome constraint on the element spacing increases the cost and complexity of the design. In addition, the array length typically needs to be notably enlarged to accommodate such physical space tapering in aperiodic arrays. To mitigate this, a new electronic space tapering method based on the E-DPCA technique is proposed for SLL reductions purposes.

The antenna phase center location, also known as the source of radiation, determines its coordinates in space. The phase center location of most single-mode antennas coincides with their geometric centers. Interestingly enough, it can be electronically displaced in multi-mode antennas [25-30]. In radar systems with moving platforms, such as synthetic aperture radar (SAR) and moving target indicator (MTI) radar, the displaced phase center antenna (DPCA) processing technique [31] is used to reduce the platform motion noise and scanning modulation noise. Traditionally, multiple identical aperture antennas were utilized to displace the antenna phase center locations and maintain its radiation pattern stationary in space [31]. The concept of displacing the phase center location in a single aperture antenna was investigated in [32-34] to create virtual arrays using multimode feed antennas. Inspired by this idea, the authors utilized the phase center displacement property of the dual-circular patches in two- and three-element arrays to establish the underlying principles of adaptive element spacing in small arrays [30].

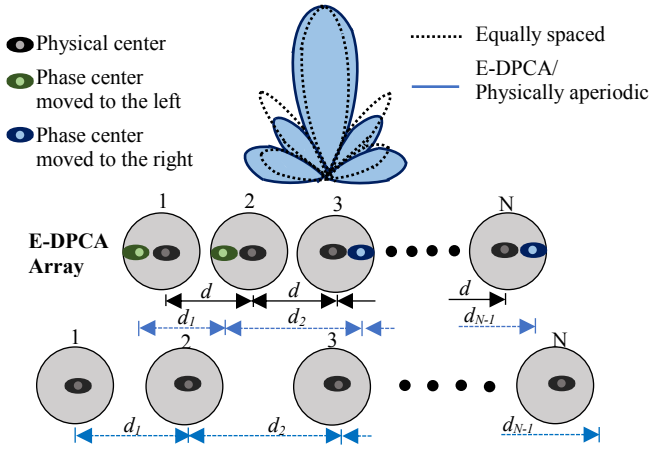

Fig. 1. Pictorial representation of the proposed N-element, equally-spaced, E-DPCA array against its physically aperiodic array counterpart with reduced SLLs. The array length in the physically aperiodic array is notably larger.

Herein, the E-DPCA technique is further investigated in N-element, equally-spaced, linear arrays to reduce their SLLs by electronically transforming them into aperiodic arrays, without having to increase the array length. Typical configurations of

Manuscript received on June xx, 2021. This work was supported in part by the National Science Foundation (NSF) CAREER Award no. ECCS-1653915 and Alabama EPSCoR Graduate Research Scholars Program (Round 15)

The authors are with the Department of Electrical and Computer Engineering, The University of Alabama in Huntsville, Huntsville, AL 35899 USA (e-mail: maria.pour@uah.edu).

the proposed E-DPCA array and physically-aperiodic array are depicted in Fig. 1, wherein comparable radiation patterns are achieved in the proposed array without any mechanical means.

In this paper, the potential of the proposed technique is explored in 9- and 21-element, equally-spaced, linear array antennas to electronically break the array periodicity and reduce side and minor lobe levels without any physical displacement. First, a brief summary of the phase center displacement property of dual-mode patch antennas, along with the resultant phase fronts and radiation patterns that transpire at the element level, is provided in Section II. The development of 9- and 21-element linear E-DPCA arrays with low SLLs is explicated in Section III. The results are then compared with the conventional techniques in Section IV. It will be demonstrated that the proposed E-DPCA technique, when coupled with the array thinning technique, facilitates further suppression of the SLLs, yet again maintaining the overall array length. For the proof of concept, the 9-element E-DPCA array is full-wave analyzed, fabricated, and tested.

II. E-DPCA Base Elements and Arrays

The phase center location of a circular patch antenna, which determines its relative coordinates in array configurations, is coincident with its physical center when only a single mode, e.g., TM_{11} or TM_{21} mode, is excited. It can be displaced away from the physical center by properly exciting the aforementioned two modes, as detailed in [25-30]. As per the cavity model, assuming the dual-mode patch is backed by an infinite ground plane, the θ-component of the electric field for a (2N+1) element uniformly-excited linear array with the x-polarized TM_{11} and TM_{21} modes is given by [25-30]:

$$E_\theta^{Total} = \sum_{n=-N}^{N} E_\theta(n)\, e^{jk_0(\, d*n \pm d_{pc}(n))sin\,\theta cos\phi + \beta(n))} \quad (1)$$

where E_θ(n) is the θ-component of the n^{th} element of the array, given by

$$E_\theta(n) = E_\theta^{TM_{11}}(n) + A_{21}(n) \times E_\theta^{TM_{21}}(n) \quad (2)$$

which can be expanded as

$$E_\theta^{TM_{11}}(n) = -j\frac{e^{-jk_0 r}}{r}\{[J_0(u_1) + J_2(u_1)]\}cos\phi \quad (3)$$

And

$$E_\theta^{TM_{21}}(n) = \frac{e^{-jk_0 r}}{r}\{[J_1(u_2) + J_3(u_2)]\}cos2\phi \quad (4)$$

where $u_1 = k_0 a_1\, sin\,\theta$ and $u_2 = k_0 a_2\, sin\,\theta$; J is the Bessel function of the first kind with associated eigenvalues of 1.8412 and 3.0542 for the TM_{11} and TM_{21} modes, respectively; a_1 and a_2 are the radii of the circular patches, exciting the TM_{11} and TM_{21} modes; A_{21} is the normalized excitation ratio (TM_{21} to TM_{11} mode), also known as the mode content factor. It is a complex number, defined as $A_{21} = |A_{21}|\angle\alpha_{21}$, where $|A_{21}|$ and α_{21} represent the magnitude and the phase shift between the two modes, respectively. The $E_\theta^{TM_{11}}$ and $E_\theta^{TM_{21}}$ radiation patterns for all (2N+1) elements in the array are assumed identical as the cavity model analysis does not take into account the mutual coupling and edge effects. The d_{pc}(n) is the phase center location of the nth dual-mode antenna element with respect to its physical center, d is the physical distance between the adjacent elements and β is the progressive phase shift of the n^{th} element in the array. As the phase center is moved away from the physical center, the adjusted electronic distance between the adjacent elements is calculated by:

$$d_e(n) = d * n + d_{pc}(n) \quad (5)$$

For the purpose of analysis, the dual-mode patch antenna in [30] is redesigned on Rogers RO3003 dielectric material and excites the TM_{11} and TM_{21} modes at the frequency of 10 GHz with probe feeds along the x-axis. The patches are stacked and positioned on 1.6mm-thick and 1mm-thick dielectric substrates with ε_r=3, backed by an infinite ground plane. The phase center displacement of the dual-mode patch antenna was detailed in [25-30], and thus a summary is provided here for brevity. Essentially, to realize the E-DPCA in a single element, while maintaining its radiation pattern stationary in space in the broadside shape, the two modes need to be excited either in-phase or out-of-phase. To attain maximum phase center displacement, the value of $|A_{21}|$ is limited to 1, resulting in maximum $d_{pc}(n)$=±0.13λ_0 phase center displacement. Some representative amplitude radiation patterns and phase distributions are plotted in Fig. 2 for different vectorial values of A_{21}. As observed, the radiation patterns remain almost unchanged, while the phase distributions undergo drastic changes, due to the non-zero A_{21} with 0° and 180° phase shifts. Of special interest is the non-zero slope of the phase patterns, implying that the phase center location of the dual-mode patch element is now moved away from its physical center. The in- and out-of-phase excitations displace the phase center along the +x and –x axes, respectively. When such E-DPCA elements are employed in an array configuration, their relative coordinates will accordingly change, altering the effective element spacing. The phase center location, *i.e.*, d_{pc} for different $|A_{21}|$ values is determined by measuring the distance the element needs to be displaced such that the slope of the E_θ phase pattern becomes uniform as detailed in [25-30].

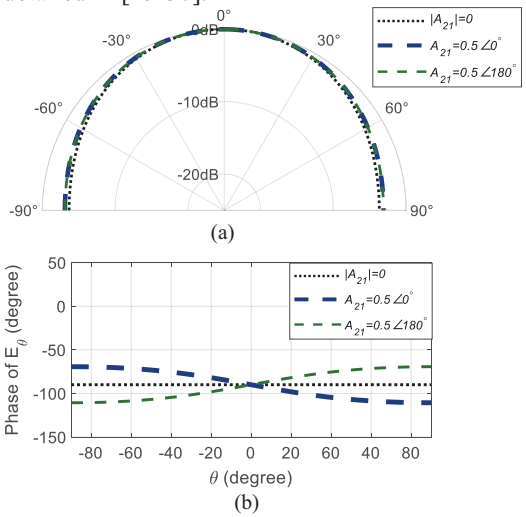

Fig. 2. Typical E-plane patterns of a dual-mode patch antenna with different vectorial values of A_{21} (a) normalized amplitude radiation patterns and (b) phase distributions.

The E-DPCA technique discussed above will be applied to 9- and 21-element, uniformly-excited, equally-spaced, linear array antennas to electronically taper the element spacing and thus breaking its periodicity to reduce SLLs without any physical displacement.

III. E-DPCA Antenna Arrays

To reduce SLLs, as opposed to conventional aperiodic arrays whose elements are physically repositioned, herein the effective electrical spacing in 9- and 21-element, uniform, linear array antennas is varied by optimally displacing the respective phase center locations of the base elements, which are the dual-mode circular patch antennas discussed in Section II. These elements are physically placed $0.7\lambda_0$ apart, where λ_0 is the free space wavelength at 10 GHz.

A. 9-Element Uniform Linear Array

The 9-element, equally-spaced, linear array antenna is symmetrically placed along the *x*-axis, as illustrated in Fig. 3. Each element has the ability to electronically displace its phase center from its physical center by $0.13\lambda_0$ on either side along the *x*-axis. Within the base elements, the phase center displacements to the right and left are color coded throughout this article and they are specified by blue and green "eye" symbols, respectively, as shown in Fig. 3. The phase centers of each element are initially considered to be placed at their respective physical centers when only the TM_{11} mode is excited, *i.e.*, $A_{21}=0\angle 0°$. This is represented by the black "eye" symbol at the center of the elements in Fig. 3. The radiation pattern generated by this configuration has a half power beamwidth (HPBW) of 8.2°, a SLL of -13.1 dB and peak gain of 17.4 dBi, per Fig. 4.

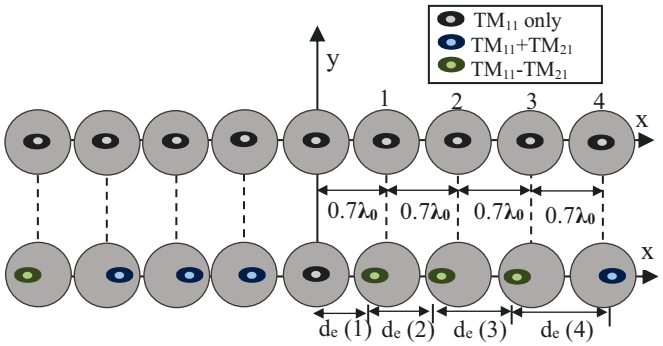

Fig. 3. Structures of the 9-element equally-spaced and the proposed E-DPCA array, whose elements are physically placed $0.7\lambda_0$ apart. The optimal tapered element spacing in the E-DPCA array, namely $d_e(1)$-$d_e(4)$, is listed in Table I.

This equally-spaced, linear array is electronically transformed into an aperiodic array by displacing the phase centers of the elements away from their physical centers, as follows. The central element of the array is considered as the reference element, whose phase center is kept at its physical center by exciting only the TM_{11} mode ($A_{21}=0\angle 0°$). The phase center displacement of the other elements in the array are symmetric about the central element placed at the origin, as depicted in Fig. 3. That is, the elements on either side excite the two modes with the same magnitude but an opposite phase shift. The optimal magnitudes of the mode content factor in the four elements on either side of the *x*-axis are $|A_{21}|_{(1)}=0.70$, $|A_{21}|_{(2)}=1$, $|A_{21}|_{(3)}=0.32$, and $|A_{21}|_{(4)}=0.94$. The first three elements along the $+x$ axis excite the higher order mode out of phase with the dominant mode, *i.e.*, $\alpha_{21}=180°$, and the two modes in the edge element are excited with $\alpha_{21}=0°$. The optimal A_{21} values are displayed on a bar graph in Fig. 5. To be consistent with the color coded "eye" symbols in Fig. 3, the in- and out-of-phase excitations within the base elements are graphically illustrated by the blue and green bars in Fig. 5. The realized electronically aperiodic array generates a modified radiation pattern with all side and minor lobe levels reduced below -17.7 dB within the observation angle of ±60°, while maintaining the 8.2° HPBW, as shown in Fig. 4. Adding the higher order TM_{21} mode to the TM_{11} mode reduces the overall gain of the array from 17.4 dBi to 16.7 dBi. As the array analysis is carried out based on the cavity model, it does not take into account the mutual coupling and edge effects and is thus considered not quite realistic for wide observation angles. Hence, the primary focus of the E-DPCA technique is placed on reducing the side and first few minor lobes within the $\theta=\pm 60°$ angular range. The effective distances between the elements in the equally-spaced and E-DPCA arrays are compared in Table I. Due to the array symmetry about the *x*-axis, A_{21} values and the distances are only provided for the right-half of the array along the $+x$ axis in Fig. 5 and Table I.

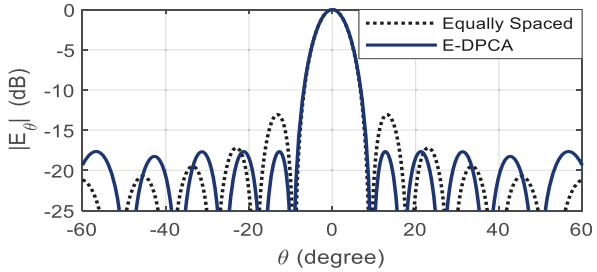

Fig. 4. Radiation patterns of 9-element linear equally-spaced (TM_{11} only) and the proposed E-DPCA array presented in Fig. 3.

The amount and direction of the phase center displacement required in each element to achieve minimum side and minor lobe levels over the angular range of ±60° is determined using the built-in genetic algorithm in MATLAB with the constraint that the maximum phase center displacement is limited to $\pm 0.13\lambda_0$ on each side, or $|A_{21}|_{max}=1$. With this E-DPCA capability, a SLL reduction of 4.6 dB is achieved in the 9-element, uniform, linear array antenna without any physical displacement.

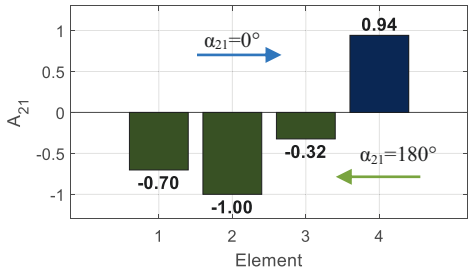

Fig. 5. Optimal A_{21} of the elements on the $+x$ axis in the 9-element linear array antenna presented in Fig. 3.

TABLE I
EFFECTIVE DISTANCES BETWEEN ADJACENT ELEMENTS FOR 9-ELEMENT LINEAR EQUALLY-SPACED AND E-DPCA ARRAYS

	Equally-Spaced (TM_{11}) SLL = -13.1 dB	**E-DPCA (TM_{11} +TM_{21}) SLL = -17.7 dB**
d_e (1) λ_0	0.7	0.60
d_e (2) λ_0	0.7	0.66
d_e (3) λ_0	0.7	0.78
d_e (4) λ_0	0.7	0.87

B. 21-Element Uniform Linear Array

In this section, the proposed concept is further examined in a 21-element linear array with the same physical spacing of $0.7\lambda_0$ and the same dual-mode elements. When only the TM_{11} mode is excited in the base elements, their respective phase centers are coincident with their physical centers, as depicted in Fig. 6 for the right-half of the array. This single-mode array generates a radiation pattern with a SLL of -13.2 dB and gain of 24 dBi, plotted in Fig. 7.

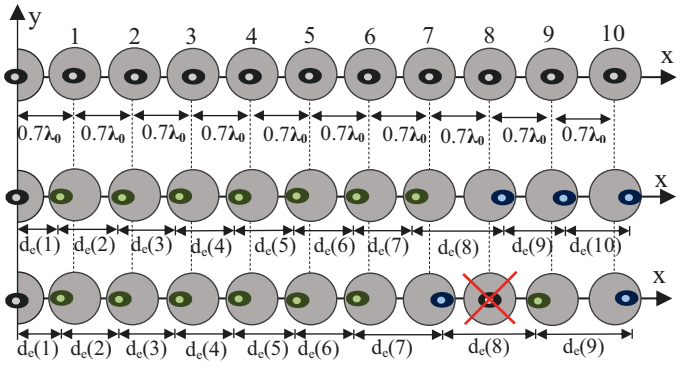

Fig. 6. Structures of the 21-element linear equally-spaced, E-DPCA and thinned arrays physically placed $0.7\lambda_0$ apart. The optimal tapered element spacing in the E-DPCA array, namely d_e (1)-d_e (10), is listed in Table II.

The phase centers of the base elements in the equally-spaced array are electronically displaced by exciting the TM_{21} modes in- and out-of-phase with the dominant TM_{11} modes to develop an aperiodic E-DPCA array with reduced SLLs. The two modes are symmetrically excited about the x-axis, similar to the 9-element E-DPCA array discussed in Section III.A. Thus, for brevity the corresponding A_{21} values for the right-half elements of the array are provided in Fig. 8. The effective distances between the phase centers of the adjacent elements in the equally-spaced and E-DPCA configurations are compared in Table II. The E-DPCA array generates a radiation pattern with all side and minor lobe levels below -15.5 dB and gain of 22.6 dBi, per Fig. 7.

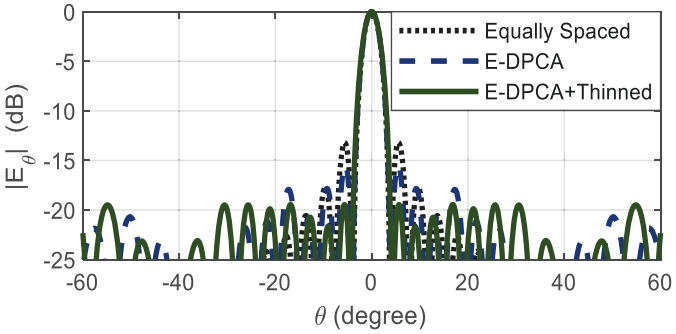

Fig. 7. Radiation patterns of 21-element linear, equally-spaced (TM_{11} only), E-DPCA and thinned antenna arrays presented in Fig. 6 with SLLs of -13.2, -15.5 and -19.5 dB, respectively.

In order to further reduce the side and minor lobe levels and increase the flexibility of this design, symmetric array thinning is performed along with the E-DPCA technique on the 21-element, equally-spaced array antenna. The MATLAB's built-in genetic algorithm was used to determine the optimal phase center locations as well as the elements that need to be turned off for the array thinning. For the thinned array geometry shown in Fig. 6, the third element from the edge on both sides of the x-axis is turned off to increase the element spacing to $1.2\lambda_0$ to further reduce the SLL. The resultant E-DPCA array reduces the side and minor lobe levels to below -19.5 dB and has a main lobe beamwidth almost identical to that of a periodic array, as observed in Fig. 7. However, the overall gain of the thinned E-DPCA array further reduces to 22 dBi. The effective distances between the phase centers of the adjacent elements of this new E-DPCA and thinned array and its corresponding A_{21} values are summarized in Table II and Fig. 8, respectively.

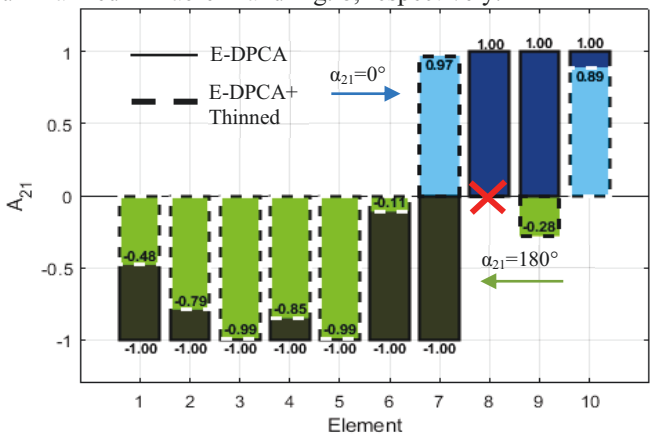

Fig. 8. Optimal A_{21} of the elements on the $+x$ axis in the 21-element linear E-DPCA and thinned arrays presented in Fig. 6.

TABLE II
EFFECTIVE DISTANCES BETWEEN ADJACENT ELEMENTS FOR 21-ELEMENT LINEAR EQUALLY-SPACED, E-DPCA AND THINNED ARRAYS

	Equally-Spaced (TM_{11}) SLL = -13.2 dB	**E-DPCA (TM_{11} +TM_{21}) SLL = -15.5 dB**	**E-DPCA+ Thinned SLL = -19.5 dB**
d_e (1) λ_0	0.7	0.55	0.62
d_e (2) λ_0	0.7	0.7	0.65
d_e (3) λ_0	0.7	0.7	0.67
d_e (4) λ_0	0.7	0.7	0.72
d_e (5) λ_0	0.7	0.7	0.68
d_e (6) λ_0	0.7	0.7	0.83
d_e (7) λ_0	0.7	0.7	0.86
d_e (8) λ_0	0.7	0.99	1.21
d_e (9) λ_0	0.7	0.7	0.87
d_e (10) λ_0	0.7	0.7	NA

Thus, from the above analyses it is concluded that element spacing can be electronically tapered to reduce SLLs in equally-spaced, uniform phased array antennas. When combined with the array thinning method, even lower SLLs can be realized without having to increase the array length or physically reposition the base elements.

IV. COMPARISON OF THE E-DPCA + THINNED ARRAYS WITH POSITION-ONLY, PHASE-ONLY AND POSITION-PHASE SYNTHESIS TECHNIQUES

In Section III, we demonstrated the capability of the proposed synthesis technique in E-DPCA arrays with adaptive element spacing to reduce SLLs without any physical displacement. To make a valid comparison of the proposed

technique with the previously-established techniques, namely phase-only [4], position-only [16], and phase-position [16], the same minimum distance of $0.5\lambda_0$ between the adjacent elements should be considered. To this end, the dielectric constant in the constitutive dual-mode circular patches discussed in Section II and [30] is increased from 3 to 4.5 to shrink the patches. The maximum phase center displacement of the base element is now restricted by $\pm 0.11\lambda_0$ on either side of the x-axis. With the miniaturized patches, the potential of the proposed technique is tested in a 21-element linear array antenna with equal element spacing of $0.5\lambda_0$, as illustrated in Fig. 9. The phase centers of the elements remain at their physical centers when only the TM_{11} mode is excited. The radiation pattern resulting from this equally-spaced linear array configuration is plotted in Fig. 10, which has a SLL of -13.2 dB and gain of 23.2 dBi.

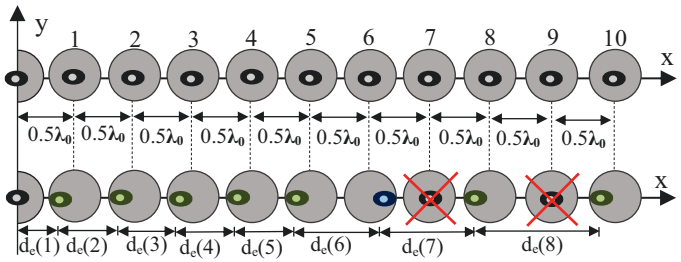

Fig. 9. Structures of the 21-element linear, equally-paced and the proposed E-DPCA + thinned arrays physically placed $0.5\lambda_0$ apart. The optimal tapered element spacing in the E-DPCA array, namely d_e (1)-d_e (8), is listed in Table III.

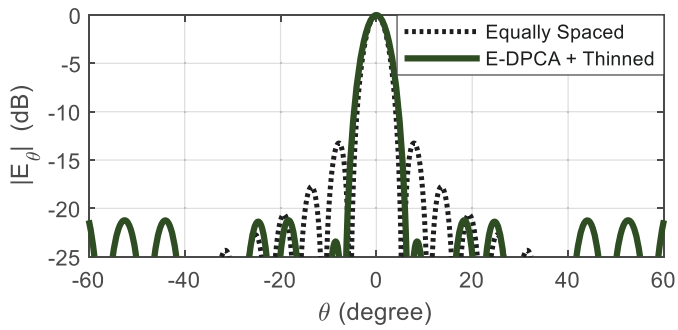

Fig. 10. Radiation patterns of 21-element linear, equally-spaced (TM_{11} only) and E-DPCA+ Thinned arrays presented in Fig. 9 with SLLs of -13.2 and -23.4 dB, respectively.

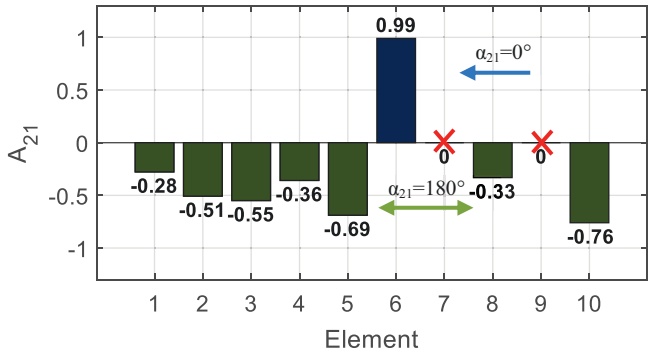

Fig. 11. Optimal A_{21} of the elements on the $+x$ axis in the 21-element thinned linear E-DPCA array presented in Fig. 9.

To break the periodicity of this configuration, the E-DPCA technique along with the array thinning is symmetrically carried out on either side of the 21-element linear array. As the two modes of the base elements are symmetrically excited along the x-axis, for brevity the phase center displacement along the $+x$-axis and their corresponding A_{21} values are shown in Figs. 9 and 11, respectively. This phase center displacement along with the array thinning creates an electronically aperiodic array with 17 elements, generating a radiation pattern with side and minor lobe levels below -21.2 dB, which is overlaid in Fig. 10. The overall gain of the thinned E-DPCA array reduces to 22.1 dBi. The effective distances between the adjacent elements in both the aforementioned configurations are summarized in Table III.

The E-DPCA and thinned array reduces the SLLs without any physical movement, while maintaining the overall array length of $10\lambda_0$. In contrast, the phase-only synthesis technique [4] when applied to the same 21-element array configuration, produces a radiation pattern with maximum sidelobe and minor lobe levels of ≈-16 dB [4]. This technique requires at least 80 elements to achieve an overall minor lobe reduction of ≈-20.1 dB, which significantly increases the overall size of the array and makes it bulky. When the position-only [16] and position-phase [16] techniques are applied to the 21-element equally-spaced antenna with a physical constraint on minimum spacing of $0.5\lambda_0$ and maximum spacing of $0.7\lambda_0$, the side and minor lobe levels reduce to -19 dB and -20 dB, respectively. However, in order to achieve the desired SLL reduction with the methods in [16], the overall array size needs to be increased to $\approx 12\lambda_0$, which is greater than that of the equally-spaced array. Moreover, none of the previously-established synthesis techniques has the ability to electronically reposition the constitutive elements without any physical displacement to generate the desired radiation patterns, as proposed in this paper. The performances of the proposed E-DPCA and thinning technique with the conventional phase-only, position-only, and position-phase techniques for the 21-element linear array are compared in Table IV. It should be mentioned that the position-only [16] and position-phase [16] techniques use the same principle of breaking the periodicity of the array without employing array thinning.

TABLE III
EFFECTIVE DISTANCES BETWEEN ADJACENT ELEMENTS FOR 21- ELEMENT LINEAR EQUALLY SPACED AND E-DPCA+ THINNED ARRAY

	Equally Spaced (TM_{11}) SLL = -13.2 dB	**E-DPCA + Thinned SLL = -21.2 dB**
d_e (1) λ_0	0.5	0.46
d_e (2) λ_0	0.5	0.47
d_e (3) λ_0	0.5	0.49
d_e (4) λ_0	0.5	0.52
d_e (5) λ_0	0.5	0.45
d_e (6) λ_0	0.5	0.75
d_e (7) λ_0	0.5	0.80
d_e (8) λ_0	0.5	0.94
d_e (9) λ_0	0.5	NA
d_e (10) λ_0	0.5	NA

TABLE IV
COMPARISON OF 21- ELEMENT LINEAR EDPCA+ THINNED ANTENNA WITH PHASE-ONLY, POSITION-ONLY, POSITION-PHASE SYNTHESIS TECHNIQUE

	Maximum minor lobe level(dB)	Array length (λ)	Element position Reconfigurability
Phase-Only Synthesis (uniform) [4]	≈-16	10	✖
Position-Only Synthesis (Non-uniform) [16]	≈-19	12	✖
Position-phase Synthesis (Non-uniform) [16]	≈-20	12	✖
Proposed E-DPCA + Thinned Array	**-21.2**	**10**	✓

It is worth noting that the E-DPCA + thinning technique can still be utilized for side and minor lobe reductions within ±60° when the main beam is scanned away from the boresight direction. As a representative example, the main beam of the 21-element equally-spaced array described above is scanned to 20° and its side and minor lobes are reduced from -13.2 dB to -17 dB using the EDPCA+ thinning technique, as shown in Fig. 12. The peak gain values are 23 dBi and 21.9 dBi for the equally-spaced and the E-DPCA + thinned arrays, respectively. The 1.1 dB gain drop is due to the presence of the second mode.

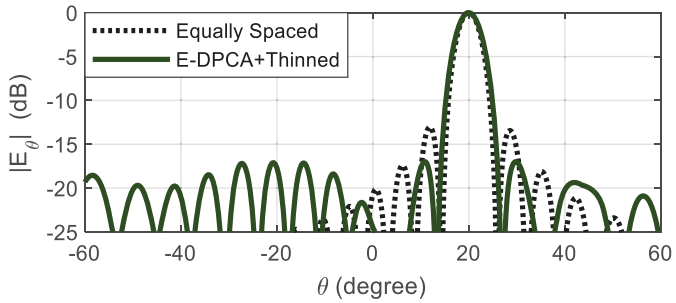

Fig. 12. Radiation patterns of 21-element linear, equally-spaced (TM_{11} only) and E-DPCA+ Thinned arrays scanned to 20° with SLLs of -13.2 and -17 dB, respectively.

As the main beam is scanned from θ=0° to 60°, the side and minor lobe reduction capability of the E-DPCA + Thinning technique gradually degrades by 5 dB (from -21 dB to -16 dB) and the overall gain drops from 22.1 dBi to 19.2 dBi. The maximum side and minor lobe reduction and the gain of the 21-elemnt E-DPCA + thinned array for different scan angles are plotted in Fig. 13. As the analysis is based on the cavity model and does not take into account the mutual coupling and edge effects, the scan angle is limited to ±60°, beyond which the radiation pattern results are not quite realistic.

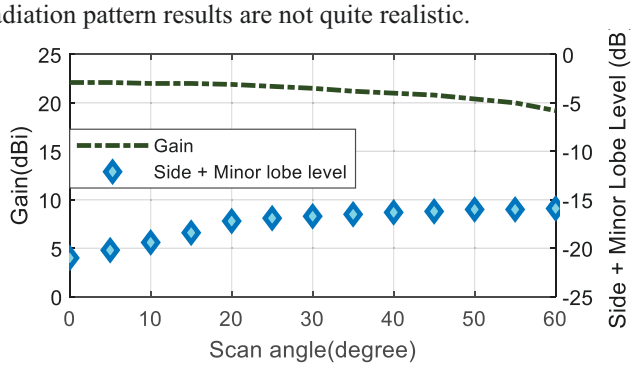

Fig. 13. Gain and side and minor lobe levels versus different scan angles for the 21-element linear, E-DPCA+ Thinned array.

It is also instructive to investigate the frequency response of the proposed E-DPCA technique as to how the SLL reductions and the array gain vary as the operating frequency changes. To this end, the 21-element, E-DPCA + thinning array is studied over the frequency range of 9.5 GHz to 10.5 GHz and the results are shown in Fig. 14. As the frequency increases, the side and minor lobe reduction capability of the E-DPCA + thinning technique reduces by about 1.3 dB and the gain variation is close to 1.6 dB. Thus, within a 10% frequency bandwidth, the E-DPCA + thinning technique achieves substantial side and minor lobe reductions without physically moving the base elements or increasing the overall length of the array.

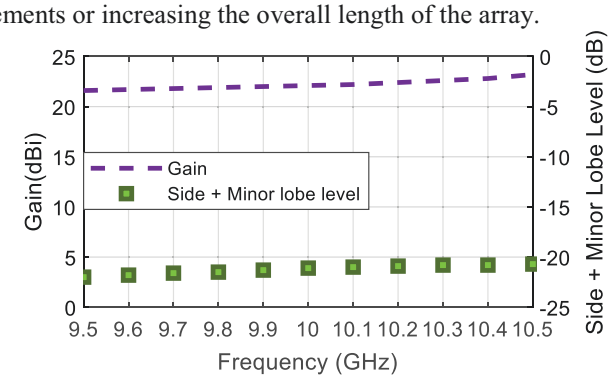

Fig. 14. Gain and side and minor lobe levels versus frequency for the 21-element linear, E-DPCA+ Thinned array.

V. EXPERIMENTAL VALIDATION OF 9-ELEMENT LINEAR ARRAY ANTENNA

The analytical results of the 9-element linear array antenna presented in Section III.A are based on the cavity model and do not take into consideration the edge effects, mutual coupling, and the probe effects. To account for all of these factors, a single-layer, 9-element linear array antenna is full-wave analyzed and designed using the finite-element based electromagnetic solver ANSYS HFSS [35]. The base elements are designed based on the single-layer, dual-mode antenna published by the authors in [30, 36]. Geometry of the 9-element linear array and its constitutive dual-mode base elements is illustrated in Fig. 15a. The 9-element linear array is printed on a 250 mm × 100mm × 1.52mm Rogers RO3003 substrate with the dielectric constant of ε_r=3. The dual-mode base elements of the array are physically placed $0.7\lambda_0$ apart (d=$0.7\lambda_0$), and are numbered *E1-E9* as presented Fig. 15a. Each element consists of a central disk and a concentric shorted annular ring, depicted in the inset of Fig. 15a, exciting the TM_{11} and TM_{21} modes at 10 GHz, respectively. The dual-mode element has the ability to displace its phase center location by $0.13\lambda_0$ away from its physical center. The 9-element linear array was fabricated using printed circuit board (PCB) technology. A photograph of the fabricated array antenna is depicted in Fig. 15b.

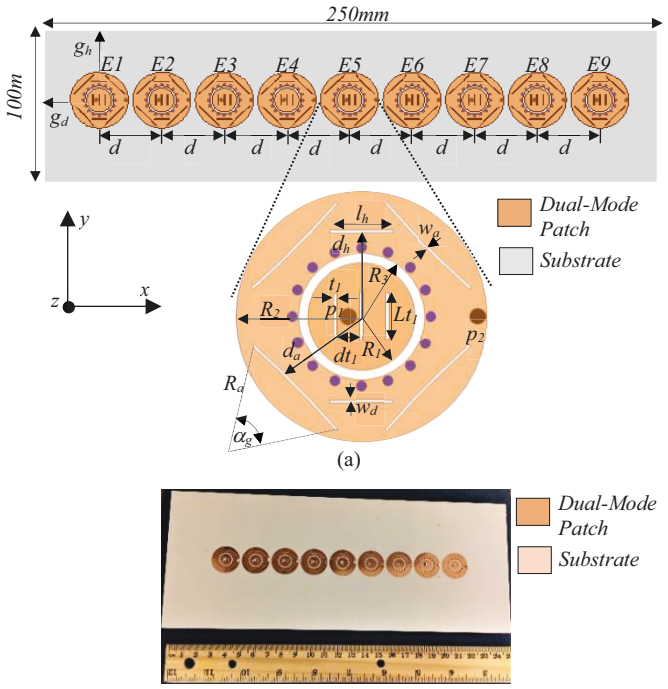

Fig. 15. (a) Illustrated geometry and (b) photograph of the 9-element linear array antenna exciting the TM_{11} and TM_{21} modes, with element spacing $0.7\lambda_0$, over a finite ground plane of 250 mm × 100 mm; the patches are etched on 1.52mm-thick Rogers RO3003 substrate with ε_r=3. (Inset: Top view of the redesigned dual-mode single-layer element based on [30, 36] with R_1=4.16 mm, R_2=9.751 mm, R_3=4.9 mm, p_1=1mm, p_2=9.035mm Lt_1=3.7 mm, t_1=0.25 mm, dt_1=2.1 mm, w_d=0.2 mm, α_g=7.6°, d_a=7.3 mm, R_a=55 mm, l_h=5.2 mm, d_h=6.5 mm, g_d=31.249 mm, and g_h=40.249 mm.)

The scattering parameters of the individual elements of the fabricated array antenna are measured using a vector network analyzer. These S-parameters include the reflection coefficients and the mutual coupling between the probes of the individual elements. The probes, denoted by p_1 and p_2 in the inset of Fig. 15.a, excite the TM_{11} and TM_{21} modes, respectively. The measured and simulated S-parameters of the central (*E5*) and edge (*E9*) elements of the 9-element array antenna are plotted in Fig. 16. As observed, the measured reflection coefficients in both the center and edge elements have been slightly shifted from 10 GHz to 9.93 GHz and 9.9 GHz, respectively. The small 0.6% and 1% errors in the frequency response of the center and edge elements, respectively, are mainly due to the manual assembly of the SMA connectors and soldering joints. Nonetheless, the measured and simulated reflection coefficients of the TM_{11} ($|S_{11}|$) and TM_{21} ($|S_{22}|$) patches of both the center and edge elements are below -10 dB at the operating frequency of 10 GHz. The measured and simulated -10 dB impedance bandwidths of the central element (E5) exciting the TM_{11} mode are 2.8% and 2.7% and those exciting the TM_{21} mode are 2% and 3.2%, respectively. The measured and simulated bandwidths of the edge element (E9) exciting the TM_{11} mode are 3% and 2.4% and those exciting the TM_{21} mode are 4% and 3.2%, respectively. The mutual coupling between the TM_{11} and the TM_{21} modes, represented by the $|S_{21}|$ in Fig. 16, is below -20 dB at 10 GHz, which is quite low.

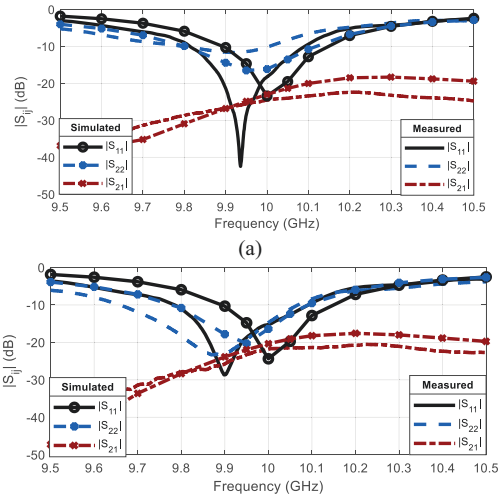

Fig. 16. Measured and simulated S-parameters of (a) center (*E5*) and (b) edge (*E9*) elements of the 9-element linear array shown in Fig. 15.

The mutual couplings between the modes in the adjacent elements of the fabricated array antenna were also measured and compared to the simulated results in Fig. 17. The maximum mutual coupling of -13 dB occurs between the TM_{21} modes in the adjacent elements of the 9-element array at 10 GHz. The mutual couplings between the TM_{11} modes as well as the TM_{11} and TM_{21} modes in the adjacent elements are around and below -20 dB, respectively. The mutual coupling between the modes of the non-adjacent elements is well below -20 dB at 10 GHz, which are omitted here for brevity.

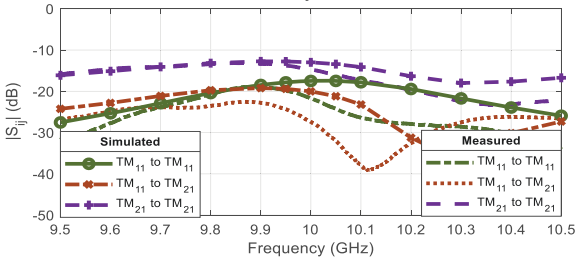

Fig. 17. Measured and simulated mutual coupling between the modes in adjacent elements of the 9-element dual-mode array antenna in Fig. 15.

Using the measured passive scattering parameters, the active reflection coefficients of the TM_{11} port in center element E5 and the TM_{11} and TM_{21} ports in edge element E9 are computed based on [37], while exciting all 18 ports of the array with their respective mode content factors. The results are plotted in Fig. 18. As observed, the -10dB impedance bandwidth of the computed active reflection coefficient of the center element E5 exciting the TM_{11} mode is 1.9%, and those of the edge element E9 exciting the TM_{11} and TM_{21} modes are 2.4% and 2.3%, respectively. Thus, the narrowest impedance bandwidth of the 9-element E-DPCA array antenna is ~2%.

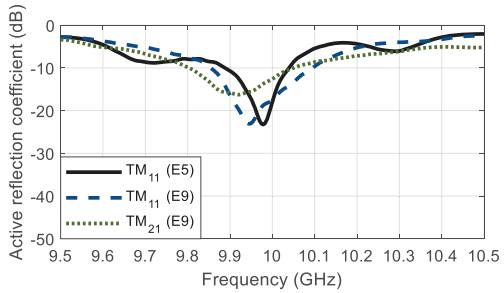

Fig. 18. Computed active reflection coefficients of the TM_{11} port in the center element (E5) and the TM_{11} and TM_{21} ports in the edge element (E9) based on the measured scattering parameters.

To validate the simulated results, the radiation pattern of the array antenna is measured using the well-established "active element pattern" technique [38,39]. The active element pattern is the radiation pattern of a single element of the array measured in the presence of all the other elements that are terminated at their characteristic impedance. The active element pattern contains the information of mutual coupling between the elements of the array and its environment and thus is different from the isolated element pattern. As all the elements in the 9-element linear array discussed above are identical and are physically equally-spaced, the overall radiation pattern of the antenna is computed using the active center element (*E5*) and edge (*E1*, *E2*, *E8*, *E9*) elements' patterns [38]. The active radiation patterns of the center and edge elements of the 9-element linear array antenna are measured individually with all the other elements terminated with 50Ω loads. For each dual-mode base element of the array, the active radiation patterns of the TM_{11} and TM_{21} modes are measured separately in the spherical near-field anechoic chamber at the University of Alabama in Huntsville. A photograph of the array antenna under test is shown in Fig. 19.

Fig. 19. A photograph of the fabricated 9-element, dual-mode linear array antenna under test in an anechoic chamber.

As a representative example, the measured active radiation patterns of the TM_{11} mode and TM_{21} modes of the center (*E5*) and edge (*E9*) elements are compared with the simulated patterns at 10 GHz in Fig. 20, which are closely aligned with each other for each mode.

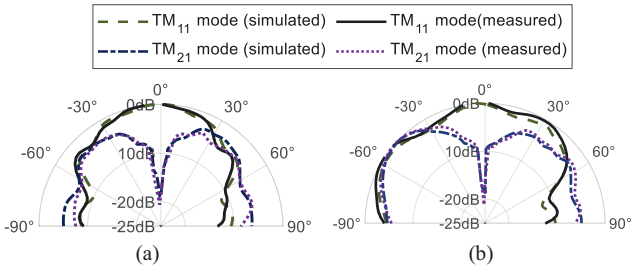

Fig. 20. Measured and simulated active radiation patterns of the (a) center (*E5*) and (b) edge (*E9*) elements at 10 GHz.

The measured active $E_\theta^{TM_{11}}$ and $E_\theta^{TM_{21}}$ radiation patterns of the center and edge elements are used to calculate the overall E_θ^{Total} radiation pattern of the 9-element array, where (2*N+1) =9, using (1). Additionally, it can be observed from Fig. 20 that the active radiation patterns of the elements are not identical due to the mutual coupling and edge effects. As the simulated and measured radiation patterns account for the mutual coupling and edge effects, the radiation patterns of the 9-element linear array antenna are shown within the observation angle of ±90°.

Initially, when only the TM_{11} modes are excited in the base elements of the 9-element linear array, it generated a pattern with a -14 dB SLL, as presented in Fig. 21a. Here the phase centers of the base elements are located at their physical centers as detailed in Section II. In order to electronically taper the element spacing and develop an E-DPCA array to reduce the sidelobe and minor lobe levels, the phase centers of the base elements are moved away from their physical centers. This is realized by varying the mode content factors A_{21}, whose optimal values and effective distances are given in Fig. 22 and Table V. Due to the mutual coupling, probes, and edge effects, the optimal A_{21} values of the full-wave analyzed array are different from those in the analytical cavity model array in Section III.A. The E-DPCA array lowers all side and minor lobe levels to -18.4 dB within the angular range of ±90° as per Fig. 21b. This 4.4 dB drop in the SLL is in accordance with the analytical results discussed in Section III.A. The measured and simulated radiation patterns for the equally-spaced, single-mode array and the proposed E-DPCA array are compared in Figs. 21a and 21b, respectively, which are in good agreement with each other and follow a similar trend.

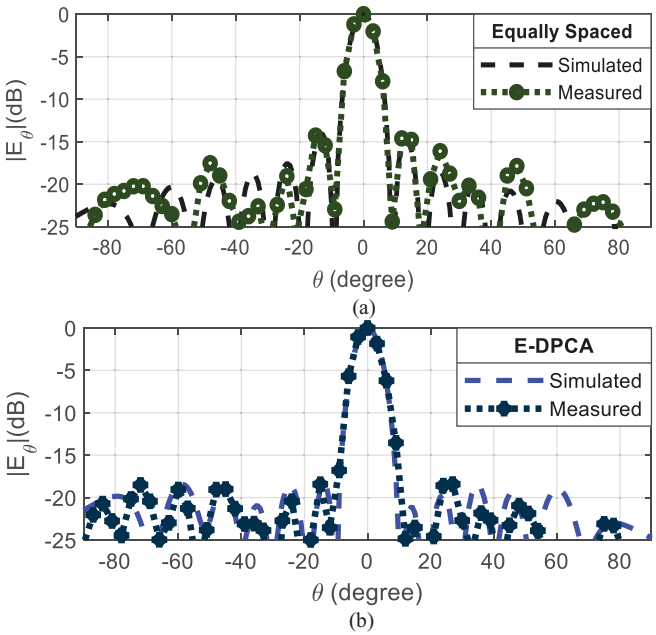

Fig. 21. Measured and simulated radiation patterns of the 9-element (a) equally-spaced (TM_{11} only) and (b) the proposed E-DPCA array.

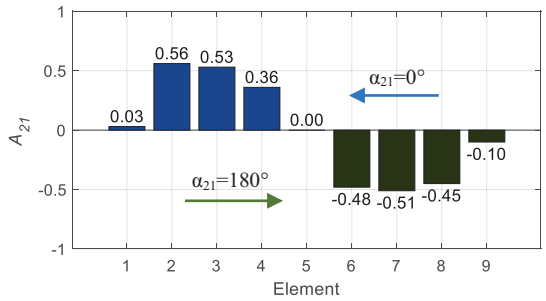

Fig. 22. Optimal A_{21} of the elements in the 9-element linear array antenna presented in Fig. 15.

TABLE V
EFFECTIVE DISTANCES BETWEEN ADJACENT ELEMENTS FOR 9-ELEMENT EQUALLY-SPACED AND E-DPCA ARRAY

	Equally Spaced (TM_{11}) SLL=-13.1dB	**E-DPCA (TM_{11} +TM_{21}) SLL=-17.7dB**
d_e (1) λ_0	0.7	0.77
d_e (2) λ_0	0.7	0.69
d_e (3) λ_0	0.7	0.67
d_e (4) λ_0	0.7	0.65
d_e (5) λ_0	0.7	0.63
d_e (6) λ_0	0.7	0.69
d_e (7) λ_0	0.7	0.71
d_e (8) λ_0	0.7	0.75

The gain values of the simulated and measured equally-spaced arrays are 16.8 dBi and 16.5 dBi, respectively, whereas, those of the E-DPCA array are 16.1 dBi and 15.5 dBi, respectively. These results confirm the proposed concept that the phase center displacement property can be applied to N-element linear array antennas to electronically transform them into aperiodic configurations to reduce their SLLs without any physical displacement, while maintaining the same overall array length. The proposed technique can potentially be applied to different linear and planar array configurations where the array radiation patterns can be modified to satisfy different requirements by electronically reconfiguring the element spacing. To fully utilize the potential of the E-DPCA-based synthesis technique in planar arrays, the base elements would need to be equipped with a two-dimensional phase center displacement capability.

VI. CONCLUSIONS

The concept of adaptively transforming N-element, linear, equally-spaced array antennas into electronically aperiodic arrays to reduce SLLs, using the E-DPCA technique, has been introduced for the first time in this paper. The proposed synthesis technique was applied to 9- and 21-element equally-spaced, linear array antennas to electronically taper the position of the constitutive elements and develop E-DPCA antennas to lower sidelobe and minor lobe levels, without any physical displacement. Compared to the conventional array synthesis techniques, this new method not only produced comparable results but also outperformed them by generating the desired pattern without any physical movement, while maintaining the overall length of the array. For the proof of concept, the 9-element array was full-wave analyzed, fabricated, and tested. The simulated and measured results were in good agreement with each other, further validating the proposed E-DPCA technique in practice for SLL reduction purposes by adaptively changing the element spacing. The proposed technique facilitates the development of flexible phased array antennas that can be electronically reconfigured over the course of operation in next-generation interference cancellers, multi-functional imaging radars, autonomous vehicles, massive multi-input multi-output (MIMO) radars, and many more.

REFERENCES

[1] C. A. Balanis, *Antenna theory: Analysis and design*, 4th Ed. Hoboken, NJ:John Wiley, 2016.
[2] G. Thadeu Freitas de Abreu and R. Kohno, "A modified dolph-chebyshev approach for the synthesis of low sidelobe beampatterns with adjustable beamwidth," *IEEE Trans. Antennas Propag.*, vol. 51, no. 10, pp. 3014-3017, Oct. 2003.
[3] A. Villeneuve, "Taylor patterns for discrete arrays," *IEEE Trans. Antennas Propag.*, vol. 32, no. 10, pp. 1089-1093, Oct. 1984.
[4] J. F. DeFord and O. P. Gandhi, "Phase-only synthesis of minimum peak sidelobe patterns for linear and planar arrays," *IEEE Trans. Antennas Propag.*, vol. 36, no. 2, pp. 191-201, Feb. 1988.
[5] Y. Aslan, J. Puskely, A. Roederer, and A. Yarovoy, "Phase-only control of peak sidelobe level and pattern nulls using iterative phase perturbations," *IEEE Antennas Wireless Propag. Lett.,* vol. 18, no. 10, pp. 2081-2085, Oct. 2019.
[6] H. Unz, "Linear arrays with arbitrarily distributed elements," *IRE Trans. Antennas Propag.*, vol. 8, no. 2, pp. 222-223, Mar. 1960.
[7] R. Harrington, "Sidelobe reduction by nonuniform element spacing," *IRE Trans. Antennas Propag.,* vol. 9, no. 2, pp. 187-192, Mar. 1961.
[8] A. Ishimaru, "Theory of unequally-spaced arrays," *IRE Trans. Antennas Propag.*, vol. 10, no. 6, pp. 691-702, Nov. 1962.
[9] D. King, R. Packard, and R. Thomas, "Unequally-spaced, broad-band antenna arrays," *IRE Trans. Antennas Propag.*, vol. 8, no. 4, pp. 380-384, July 1960.
[10] M. Andreasen, "Linear arrays with variable interelement spacings," *IRE Trans. Antennas Propag.*, vol. 10, no. 2, pp. 137-143, Mar. 1962.
[11] K. Tomiyasu, "Combined equal and unequal element spacings for low sidelobe pattern of a symmetrical array with equal-amplitude elements," *IEEE Trans. Antennas Propag.*, vol. 39, no. 2, pp. 265-266, Feb. 1991.
[12] W. Zhang, L. Li, and F. Li, "Reducing the number of elements in linear and planar antenna arrays with sparseness constrained optimization," *IEEE Trans. Antennas Propag.*, vol. 59, no. 8, pp. 3106-3111, Aug. 2011.
[13] S. Chatterjee and S. Chatterjee, "Pattern synthesis of center fed linear array using Taylor one parameter distribution and restricted search Particle Swarm Optimization," *J. Commun. Technol. Electron.,* vol. 59, no. 11, pp. 1112-1127, 2014.
[14] C. Zhang, X. Fu, L. P. Ligthart, S. Peng, and M. Xie, "Synthesis of broadside linear aperiodic arrays with sidelobe suppression and null steering using whale optimization algorithm," *IEEE Antennas Wireless Propag. Lett.*, vol. 17, no. 2, pp. 347-350, Feb. 2018.
[15] B. P. Kumar and G. R. Branner, "Design of unequally spaced arrays for performance improvement," *IEEE Trans. Antennas Propag.*, vol. 47, no. 3, pp. 511-523, Mar. 1999.
[16] D. G. Kurup, M. Himdi, and A. Rydberg, "Synthesis of uniform amplitude unequally spaced antenna arrays using the differential evolution algorithm," *IEEE Trans. Antennas Propag.,* vol. 51, no. 9, pp. 2210-2217, Sept. 2003.
[17] S. K. Goudos, K. Siakavara, T. Samaras, E. E. Vafiadis, and J. N. Sahalos, "Sparse linear array synthesis with multiple constraints using differential evolution with strategy adaptation," *IEEE Antennas Wireless Propag. Lett.*, vol. 10, pp. 670-673, 2011.
[18] S. Caorsi, A. Lommi, A. Massa, and M. Pastorino, "Peak sidelobe level reduction with a hybrid approach based on GAs and difference sets," *IEEE Trans. Antennas Propag.*, vol. 52, no. 4, pp. 1116-1121, April 2004.
[19] B. Fuchs, A. Skrivervik and J. R. Mosig, "Synthesis of uniform amplitude focused beam arrays," *IEEE Antennas Wireless Propag. Lett.*, vol. 11, pp. 1178-1181, 2012
[20] D. Pinchera, M. D. Migliore and G. Panariello, "Synthesis of large sparse arrays using IDEA (Inflating-Deflating Exploration Algorithm)," *IEEE Trans. Antennas Propag.*, vol. 66, no. 9, pp. 4658-4668, Sept. 2018.

[21] R. L. Haupt, "Thinned arrays using genetic algorithms," *IEEE Trans. Antennas Propag.*, vol. 42, no. 7, pp. 993-999, July 1994.
[22] R. Willey, "Space tapering of linear and planar arrays," *IRE Trans. Antennas Propag.*, vol. 10, no. 4, pp. 369-377, July 1962.
[23] O. Quevedo-Teruel and E. Rajo-Iglesias, "Ant colony optimization in thinned array synthesis with minimum sidelobe level," *IEEE Antennas Wireless Propag. Lett*., vol. 5, pp. 349-352, 2006.
[24] X. Wang, Y. Jiao, and Y. Tan, "Synthesis of large thinned planar arrays using a modified iterative fourier technique," *IEEE Trans Antennas Propag*., vol. 62, no. 4, pp. 1564-1571, April 2014
[25] Z. A. Pour, "Control of phase center and polarization in circular microstrip antennas," Master of Science thesis, University of Manitoba, Winnipeg, Canada, July 2006.
[26] L. Shafai and Z. A. Pour, "Displacement of phase center location in circular microstrip antennas," *Microw. Opt. Technol. Lett*, Vol. 50, No. 10, pp. 2531-2535, Oct. 2008.
[27] Z. A. Pour and L. Shafai, "Control of phase center and polarization in circular microstrip antennas," *2006 IEEE Antennas Propag. Soc. Int. Symp.*, Albuquerque, NM, pp. 1441-1444, 2006.
[28] Z. A. Pour and L. Shafai, "Adaptive aperture antennas with adjustable phase centre locations," *2012 IEEE Int. Workshop on Antenna Technol*. (iWAT), Tucson, AZ, pp. 355-357, 2012.
[29] Z. A. Pour, L. Shafai, and A. M. Mehrabani, "Virtual array antenna with displaced phase centers for GMTI applications," *2011 IEEE RadarCon (RADAR)*, Kansas City, MO, pp. 830-834, 2011.
[30] T. Mitha and M. Pour, "Principles of Reconfigurable Element Spacing Linear Array Antennas," *Sci Rep*, vol 11, pp. 5584, 2021.
[31] M. I. Skolnik, *Radar Handbook*, New York:McGraw-Hill, 1990.
[32] L. Shafai, S. K. Sharma, B. Balaji, A. Damini and G. Haslam, "Multiple phase center performance of reflector antennas using a dual mode horn," *IEEE Trans. Antennas Propag.,* vol. 54, no. 11, pp. 3407-3417, Nov. 2006.
[33] Z. A. Pour and L. Shafai, "Investigation of virtual array antennas with adaptive element locations and polarization using parabolic reflector antennas*," IEEE Trans. Antennas Propag*., vol. 61, no. 2, pp. 688-699, Feb. 2013.
[34] Z. A. Pour and L. Shafai, "Improved cross-polarization performance of a multi-phase-center parabolic reflector antenna," *IEEE Antennas Wireless Propag. Lett.,* vol. 13, pp. 540-543, 2014.
[35] *High Frequency Structure Simulator* (HFSS 20.0). Canonsburg, PA, USA, ANSYS, 2020.
[36] Z. Iqbal, T. Mitha, and M. Pour, "A self-nulling single-layer dual-mode microstrip patch antenna for grating lobe reduction," *IEEE Antennas Wireless Propag. Lett*., vol. 19, no. 9, pp. 1506-1510, Sept. 2020.
[37] D. M. Pozar, "A relation between the active input impedance and the active element pattern of a phased array," *IEEE Trans. Antennas Propag*., vol. 51, no. 9, pp. 2486-2489, Sept. 2003.
[38] D. M. Pozar, "The active element pattern," *IEEE Trans. Antennas Propag*., vol. 42, no. 8, pp. 1176-1178, Aug. 1994.
[39] D. F. Kelley and W. L. Stutzman, "Array antenna pattern modeling methods that include mutual coupling effects," *IEEE Trans. Antennas Propag*., vol. 41, no. 12, pp. 1625-1632, Dec. 1993.

Tanzeela H. Mitha was born in Pune, India in 1993. She received her B.E in Electronics and Telecommunication from University of Pune, Maharashtra, India in 2016. She received her Masters of Science degree in electrical engineering from The University of Alabama in Huntsville, Alabama, USA in 2018. She is presently a Ph.D. student at The University of Alabama in Huntsville, working with Dr. Maria Pour. Her research interests include microstrip patch antennas, wideband antennas, dual-mode antennas and phased array antennas.

Maria Pour (S'06–M'11–SM'16) received the Ph.D. degree in electrical engineering from the University of Manitoba, Winnipeg, MB, Canada, in 2012. She is an Associate Professor with the Department of Electrical and Computer Engineering, The University of Alabama in Huntsville, AL, USA. She has coauthored six book chapters and has published over 90 journal articles and conference proceedings. Her research interests are in the areas of applied electromagnetics and antennas, including phased array antennas, multi-mode antennas, wideband reconfigurable antennas, virtual aperture antennas, reflector antennas and feeds, primary matched feeds, and antenna measurement techniques.

Dr. Pour received the 2017 CAREER Award from the U.S. National Science Foundation. She was named as the 2017 Outstanding Junior Faculty and the 2017 Outstanding Research Faculty by the College of Engineering, The University of Alabama in Huntsville. She was the recipient of the 2020 Outstanding Teaching Award of the College of Engineering and the 2021 Joseph Dowdle Outstanding Faculty Award of the Department of Electrical and Computer Engineering, The University of Alabama in Huntsville. She has been serving as an Associate Editor for the IEEE TRANSACTIONS ON ANTENNAS AND PROPAGATION and the IEEE ANTENNAS AND WIRELESS PROPAGATION LETTERS, since 2016 and 2020, respectively.